Science & Technology Development Journal – Engineering and Technology 2023, 5(SI2):24-32

Open Access Full Text Article

Research Article

Analysis of cracked Reissner-Mindlin plate using an extended meshfree method

Vay Siu Lo[1,2], Thien Tich Truong[1,2], Nha Thanh Nguyen[1,2,*]

ABSTRACT

An extended meshfree method for analyzing cracked plates based on Reissner-Mindlin theory is presented in this paper. Among a variety of meshfree formulations, the radial point interpolation method (RPIM) is chosen in this study due to the satisfaction of the Kronecker delta property. The essential boundary conditions, therefore, are easily imposed in the RPIM. The shape function derived from RPIM is employed to interpolate the field variables. An extended RPIM formulation is used to model the crack segment without explicitly defining it in the discretized domain. The discontinuity due to the crack is defined by extrinsic enriched functions, particularly, the jump in the displacement field on two sides of the crack is modelled by the Heaviside function, and the stress singularity near the crack tip is described by the asymptotic enriched function. In this study, the stress resultant intensity factors (SRIFs) are evaluated through the interaction integral approach. The obtained SRIFs are shown in the paper through many numerical examples for comparison purposes. The trending variation of SRIFs is also observed from the numerical results. It can be remarked that the SRIFs depend on many factors: the number of cracks, crack orientation, load type and boundary conditions. The numerical examples show the accuracy of the present approach. The obtained results are compared with analytical solutions and other numerical methods.

Key words: cracked plate, Reissner-Mindlin plate, extended meshfree method, XRPIM

[1]*Department of Engineering Mechanics, Faculty of Applied Sciences, Ho Chi Minh City University of Technology (HCMUT), 268 Ly Thuong Kiet Street, District 10, Ho Chi Minh City, Vietnam.*

[2]*Vietnam National University Ho Chi Minh City, Linh Trung Ward, Thu Duc City, Ho Chi Minh City, Vietnam.*

Correspondence

Nha Thanh Nguyen, Department of Engineering Mechanics, Faculty of Applied Sciences, Ho Chi Minh City University of Technology (HCMUT), 268 Ly Thuong Kiet Street, District 10, Ho Chi Minh City, Vietnam.

Vietnam National University Ho Chi Minh City, Linh Trung Ward, Thu Duc City, Ho Chi Minh City, Vietnam.

Email: nhanguyen@hcmut.edu.vn

History

- Received: 16-12-2022
- Accepted: 24-8-2023
- Published Online: 31-12-2023

DOI :

https://doi.org/10.32508/stdjet.v6iSI2.1066

INTRODUCTION

Many engineering applications involve thin plate structures, such as civil, automobile, ship and other mechanical systems. Hence, it is essential to analyze the behavior of plate structures. For the numerical computation of plate structures, using a plate formulation, such as Kirchhoff-Love theory[1–4], Reissner-Mindlin theory[5–8], higher-order shear deformation theory (HSDT)[9–11] and so on requires less number of degrees of freedom (DOFs) than considering it as a 3D solid model. Hence, the computational cost for modelling plate structures is reduced when using a plate formulation. The Reissner-Mindlin theory is a simple plate formulation that considers first-order shear deformation and is appropriate for moderately thick plates. With a C^0 continuity formulation, it does not require higher-order shape functions.

Fracture analysis is also a crucial aspect besides the analysis of plate structures since it affects the durability of the structures. Therefore, more studies on the modelling of plates with through thickness crack are necessary. Many approaches have already been developed for solving cracked plate bending problems using Reissner-Mindlin theory[12–14], Kirchhoff-Love theory[15,16] and HSDT[17,18].

The eXtended Finite Element Method (XFEM) is a powerful technique for modeling crack discontinuity without explicitly defining it in the problem geometry and simulating crack growth without remeshing, which was first proposed by[19] and has been widely applied. In the XFEM formulation, the enrichment functions are used to describe the discontinuity in displacement fields across the crack faces and the singularity in stress fields near the crack tip.

Besides the conventional mesh-based finite element method, the meshfree method is a developing branch of computational method. The Radial Point Interpolation Method (RPIM)[20,21] is a meshfree method that has a special property called the Kronecker delta. This makes it easy to apply the essential boundary conditions in the RPIM, unlike many other meshfree methods. For that reason, the RPIM is chosen in this study. In the same way as formulating XFEM, Nguyen *et al.* combined RPIM and the extended formulation with enrichment functions to introduce XPRIM, which they used for 2D fracture problems[22–24]. However, there are still few studies on fracture analysis of cracked plates using XRPIM. In the scope of this study, cracked Reissner-Mindlin plates is analyzed by using the XRPIM.

The stress resultant intensity factors (SRIFs) of Reissner-Mindlin plates with through-thickness crack

Cite this article : Lo V S, Truong T T, Nguyen N T. **Analysis of cracked Reissner-Mindlin plate using an extended meshfree method**. *Sci. Tech. Dev. J. – Engineering and Technology* 2024; 5(SI2):24-32.

are evaluated in this paper. The XRPIM is used for modeling, and the radial basis to construct the shape function is the Thin Plate Spline (TPS) function. The accuracy of the proposed method is verified by various numerical tests, showing the effectiveness of the approach.

METHODOLOGY

Reissner-Mindlin plate

The first-order transverse shear deformation is considered in the Reissner-Mindlin theory, so the plate cross-section the after deformation is still straight but not normal to the mid-surface[25]. In the Cartesian coordinate (see Fig. 1), the displacement components are defined as the following equations

$$\begin{cases} u_1(x_1,x_2,x_3) = x_3\varphi_1(x_1,x_2) \\ u_2(x_1,x_2,x_3) = x_3\varphi_2(x_1,x_2) \\ u_3(x_1,x_2,x_3) = w(x_1,x_2) \end{cases} \quad (1)$$

where (x_1,x_2,x_3) is the position of the interest point, w is the deflection, φ_1 and φ_2, in that order, are the rotation angle about x_2 and x_1 axes. The sign convention for φ_1 and φ_2 is depicted in Fig. 1.

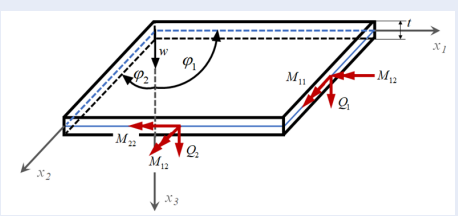

Figure 1: Deflection, rotations and resultants of a plate

In plate formulation, the constitutive relation for an isotropic homogenous material is given as[12]

$$M = \begin{bmatrix} M_{11} \\ M_{22} \\ M_{33} \end{bmatrix} = \frac{Et^3}{12(1-v^2)} \times \begin{bmatrix} 1 & v & 0 \\ v & 1 & 0 \\ 0 & 0 & \frac{1-v}{2} \end{bmatrix} \begin{bmatrix} \varphi_{1,1} \\ \varphi_{2,2} \\ \varphi_{1,2}+\varphi_{2,1} \end{bmatrix} = \frac{t^3}{12} D_b \varepsilon_b \quad (2)$$

$$Q = \begin{bmatrix} Q_1 \\ Q_2 \end{bmatrix} = \kappa t \begin{bmatrix} \mu & 0 \\ 0 & \mu \end{bmatrix} \begin{bmatrix} \varphi_1 + w_{,1} \\ \varphi_2 + w_{,2} \end{bmatrix} = \kappa t D_s \varepsilon_s \quad (3)$$

where M denotes the moment resultants and Q stands for the shear force resultants, E is the Young's modulus, μ is the shear modulus, v is the Poisson ratio, t is plate thickness and t is the shear correction factor and takes the value as 5/6[12]. ε_b and ε_s indicate the strain due to bending and shear, respectively.

In the above equations, D_b and D_s, in that order, are the bending stiffness tensor and shear stiffness tensor, and defined as

$$D_b = \frac{E}{(1-v^2)} \begin{bmatrix} 1 & v & 0 \\ v & 1 & 0 \\ 0 & 0 & \frac{1-v}{2} \end{bmatrix} \quad (4)$$

$$D_s = \begin{bmatrix} \mu & 0 \\ 0 & \mu \end{bmatrix} \quad (5)$$

The stiffness matrix of the Reissner-Mindlin plate is derived from the weak formulation and expressed as[26]

$$K = \frac{t^3}{12} \int_\Omega B_b^T D_b B_b d\Omega + \int_\Omega B_s^T D_s B_s d\Omega \quad (6)$$

As seen in the equation, the stiffness matrix is made up of two parts: bending (the first term on the right-hand side) and shear components (the second term). B-operators are defined as follow

$$B_b^I = \begin{bmatrix} 0 & \phi_{I,1} & 0 \\ 0 & 0 & \phi_{I,2} \\ 0 & \phi_{I,2} & \phi_{I,1} \end{bmatrix} \quad (7)$$

$$B_s^I = \begin{bmatrix} \phi_{I,1} & \phi_I & 0 \\ \phi_{I,2} & 0 & \phi_I \end{bmatrix} \quad (8)$$

here ϕ_I denotes the shape function. And in this paper, as indicated in the Introduction section, the shape function is derived from the RPIM. More detail of the construction of RPIM shape function can be found in the reference[27].

For brevity, the RPIM shape function consists of two constituents: a radial basis and a polynomial basis. In this study, the Thin Plate Spline (TPS) function is employed as the radial basis to form the shape function and is defined below

$$R_i(x_1,x_2) = r_i^\eta \quad (9)$$

where η is the shape parameter, r_i is the distance between the interest point x and the node x_i, and defined as

Extended Radial Point Interpolation Method

Fig. 2 shows different sets of nodes in a cracked plate problem. W contains all nodes in the support domain (includes grey, blue and red dots in Fig. 2). W_s contains nodes whose support domain is cut by the crack (blue dots in Fig. 2). And W_t is the set of nodes in which the support domain contains crack tip (red dots in Fig. 2).

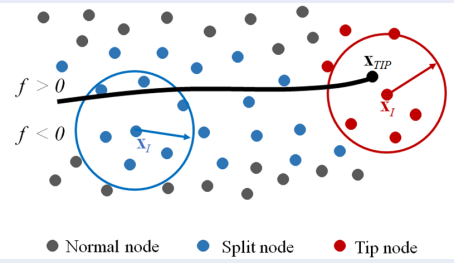

Figure 2: Type of enriched nodes and their support domains

In the "extended" concept, the interpolation function for an interest point x is incorporated with the enriched function and expressed as below

$$w^h(x) = \sum_{i\in W} \phi_i(x) w_i + \sum_{j\in W_s} \phi_j(x)\left(H - H_j\right) b_j^w + \sum_{k\in W_t} \phi_k(x)\left[\sum_{l=1}^{4}\left(G_l - G_{lk}\right) c_{lk}^w\right]$$

$$\varphi^h(x) = \sum_{i\in W} \phi_i(x) \varphi_i + \sum_{j\in W_s} \phi_j(x)\left(H - H_j\right) b_j^\varphi + \sum_{k\in W_t} \phi_k(x)\left[\sum_{l=1}^{4}\left(F_l - F_{lk}\right) c_{lk}^\varphi\right] \quad (10)$$

in which H denotes the Heaviside function and is defined as the following equation

$$H(f(x)) = \begin{cases} +1 \; if \; f(x) > 0 \\ -1 \; if \; f(x) < 0 \end{cases} \quad (11)$$

In Eqs. (10) and (11), the asymptotic enrichment functions F_l and G_l are defined as [12]

$$F_l = (r,\theta) = \{\sqrt{r}\sin\frac{\theta}{2}, \sqrt{r}\cos\frac{\theta}{2}, \sqrt{r}\sin\frac{\theta}{2}\sin\theta, \sqrt{r}\cos\frac{\theta}{2}\sin\theta\} \quad (12)$$

$$G_l = (r,\theta) = \{r^{3/2}\sin\frac{\theta}{2}, r^{3/2}\cos\frac{\theta}{2}, r^{3/2}\sin\frac{3\theta}{2}, r^{3/2}\cos\frac{3\theta}{2}\} \quad (13)$$

where r is the distance from the interest point x to the crack tip x_{TIP}, θ denotes the angle made up of the crack segment and the line connecting the interest point x and the crack tip x_{TIP}.

As can be seen from Eqs. (13) and (14), F_l is the enrichment functions for the bending components appearing in the interpolation equation of the rotation angle. F_l contains terms proportional to $r^{1/2}$. G_l is the enrichment functions for the shear components appearing in the equation of deflection. G_l contains terms proportional to $r^{3/2}$.

In order to compute the stiffness matrix as in Eq (6), the B-operator is now including the standard $B^{standard}$ and enriched $B^{enriched}$ components, namely

$$B = \left[B^{standard}, B^{enriched}\right] \quad (14)$$

The enriched B-operators for bending component are given as

$$B_b^{spit\ enr} = \begin{bmatrix} 0 & [\phi_I(H-H_I)]_{,1} & 0 \\ 0 & 0 & [\phi_I(H-H_I)]_{,2} \\ 0 & [\phi_I(H-H_I)]_{,2} & [\phi_I(H-H_I)]_{,1} \end{bmatrix} \quad (15)$$

$$B_b^{TIP\ enr,l} = \begin{bmatrix} 0 & [\phi_I(F-F_I)]_{,1} & 0 \\ 0 & 0 & [\phi_I(F-F_I)]_{,2} \\ 0 & [\phi_I(F-F_I)]_{,2} & [\phi_I(F-F_I)]_{,1} \end{bmatrix} \quad (16)$$

And for shear component

$$B_S^{spit\ enr} = \begin{bmatrix} [\phi_I(H-H_I)]_{,1} & [\phi_I(H-H_I)]_{,2} \\ \phi_I(H-H_I) & 0 \\ 0 & \phi_I(H-H_I) \end{bmatrix}^T \quad (17)$$

$$B_s^{tip\ enr,l} = \begin{bmatrix} [\phi_I(G_l-G_{lI})]_{,1} & [\phi_I(G_l-G_{lI})]_{,2} \\ \phi_I(F_l-F_{lI}) & 0 \\ 0 & \phi_I(F_l-F_{lI}) \end{bmatrix} \quad (18)$$

Stress resultant intensity factors

To evaluate the fracture behavior of cracked plates, the factors of stress resultant intensity (SRIFs) are important characteristics that need to be defined. SRIFs are defined as the following equation [25]

$$\begin{cases} K_1 = \lim\limits_{r\to 0}\sqrt{2r}M_{22}(r,0) \\ K_2 = \lim\limits_{r\to 0}\sqrt{2r}M_{12}(r,0) \\ K_3 = \lim\limits_{r\to 0}\sqrt{2r}Q_2(r,0) \end{cases} \quad (19)$$

where K_1 and K_2 are the factors of moment intensity and K_3 is the factor of shear force intensity.

The stress intensity factors (SIFs) in 3D elasticity are derived by the following relation [25]

$$\begin{cases} k_1(x_3) = \dfrac{12x_3}{t^3}K_1 \\ k_2(x_3) = \dfrac{12x_3}{t^3}K_2 \\ k_3(x_3) = \dfrac{3}{2t}\left[1-\left(\dfrac{2x_3}{t}\right)^2\right]K_3 \end{cases} \quad (20)$$

The values of SRIFs are calculated from the interaction integral, more detail can be found in references [28]. The interaction integral for the cracked plate is defined as the following expression

$$I = \int_A (M_{ij}\varphi_{i,1}^{aux} + M_{ij}^{aux}\varphi_{i,1} + Q_j w_{i,1}^{aux} + Q_j^{aux} w_{,1} - W^{int}\delta_{1j})q_{,j}dA + \int_A [\left(M_{ij,j}^{aux} - Q_i^{aux}\right)\varphi_{i,1} + Q_i\left(\varphi_{i,1}^{aux} + w_{,i1}^{aux} + \varepsilon_{si,1}^{aux}\right)]qdA - \int_A p w_{,1}^{aux} q dA \quad (21)$$

where "aux" is the abbreviation of the "auxiliary" state, weight function q is defined as

$$q = \left(1 - 2\frac{|x_1 - x_1^{tip}|}{c}\right)\left(1 - 2\frac{|x_2 - x_2^{tip}|}{c}\right) \quad (22)$$

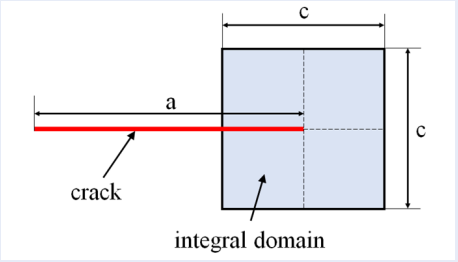

Figure 3: Interaction integral domain

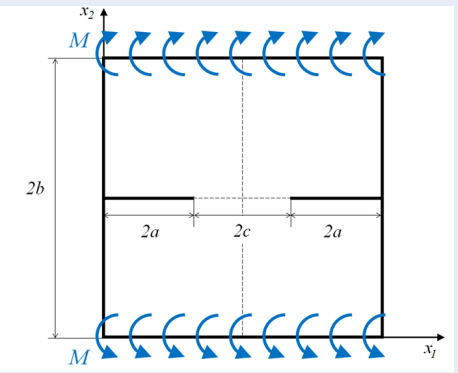

Figure 4: Plate with two cracks on opposite edges.

In Eq. (23), c is the side length of integral domain as shown in Fig. 3.

After computing the interaction integral I, the SRIFs are derived by using the following relation

$$I^{(1,2,3)} = \frac{24\pi}{Et^3}\left(K_1 K_1^{aux} + K_2 K_2^{aux}\right) + \frac{12\pi}{10\mu t} K_3 K_3^{aux} \quad (24)$$

For example, K_1 is obtained by setting $K_1^{aux} = 1$, $K_2^{aux} = K_3^{aux} = 0$.

NUMERICAL RESULTS

There are two numerical examples in this section, and each example contains two problems, particularly:

- Square plate with two edge-cracks.
- Square plate with inclined central crack.

In each example, there are two types of loads considered: distributed moment and uniform pressure. The stress resultant intensity factors are computed in each problem, and the variation of SRIFs with respect to different crack orientations and crack lengths is also examined.

Square plate with two edge-cracks

Distributed bending moment on opposite edges

In this example, a square plate with the dimensions of $2b$ = 2 m and thickness t is examined. The plate contains two cracks on two opposite edges and is subjected to distributed bending moment M on the other two edges (see Fig. 4). The crack length is $2a$, and the distance between the two crack tips is $2c = 2b - 4a$. The material properties are: Young's modulus E=1000 Pa and Poisson ratio $v = 0.3$. The discretized model with 40×40 nodes is used in this example.

Figure 5 presents the variation of the normalized SRIF $K_1/(M\sqrt{a})$ versus various ratios c/b. The results are shown for two cases: b/t = 2 and b/t = 6. The current XRPIM results are compared with the analytical solution [29], showing good agreement.

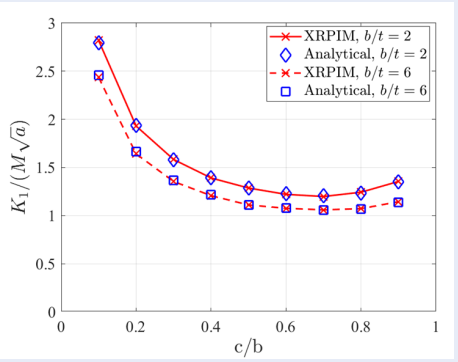

Figure 5: Normalized K_1 with different c/b ratios of two cases: b/t = 2 and b/t = 6

Several observations can be drawn from Fig. 5: thicker plate has higher SRIF, the SRIF in both cases tends to decrease as the c/b ratio increases from 0.1 to 0.7, and after that the SRIF slightly increases when the c/b ratio is in the range of 0.7 – 0.9. It should be noted that a decrease in c/b ratio means an increase in the crack length, so the result can be interpreted as when the crack length increases, the SRIF also increases.

Transverse uniform pressure

In the second load case, the plate is subjected to transverse uniform pressure p. The plate is now simply supported on top and bottom edges (two edges without cracks), see Fig. 6. The crack length is a, and the distance between the two crack tips is $2c = 2b - 2a$. The material properties are the same as the first problem: E=1000 Pa and $v = 0.3$. This model is also discretized into a set of 40×40 scattered nodes.

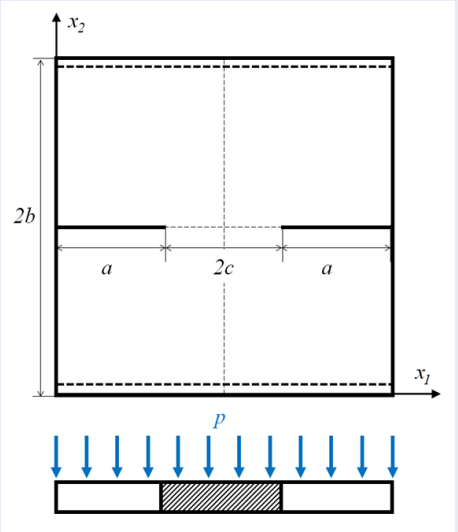

Figure 6: Simply supported plate with two edge cracks subjected to uniform pressure.

Figure 7 presents the variation of the normalized SRIF $K_1/\left(pb^2\sqrt{a}\right)$ with respect to different c/b ratios. The results are shown for two cases: b/t = 2 and b/t = 6. The current XRPIM results are compared with DBEM [30], showing good agreement.

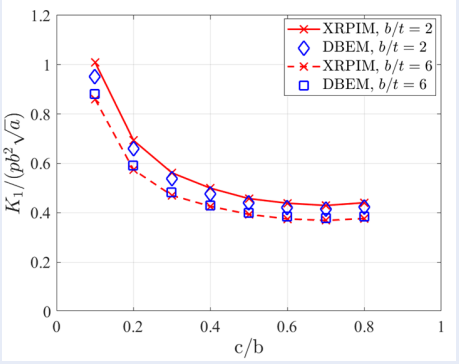

Figure 7: Normalized K_1 with different *c/b* ratios

Similar to the first example, some observations can be drawn from Fig. 7: the smaller the *b/t* ratio, the higher the SRIF. The SRIF in both cases tends to decrease as the *c/b* ratio increases from 0.1 to 0.7, and after that the SRIF slightly increases.

Square plate with inclined central crack

Distributed bending moment on two opposite edges

This example analyzes a square plate with dimension 2*b* containing an inclined crack at the center, see Fig. 8. The crack length is 2*a*. The plate is subject to distributed moment M on top and bottom edges. The material properties are given as follows: E = 1000 Pa and $v = 0.3$. The discretized model with 50×50 nodes is used.

The moment intensity factors K_1 and K_2 are computed in the XRPIM approach and compared with the analytical solutions [31]

$$K_1 = \phi\,(t/a)\,M\sqrt{a}\cos^2\beta,$$
$$K_2 = \psi\,(t/a)\,M\sqrt{a}\cos\beta\sin\beta. \quad (25)$$

where β is the inclination angle (see Fig. 8). The values of coefficients ϕ, ψ can be referred to [32]. For 2*a* = 2 m, *b/t* = 5 and *t/a* = 1, these coefficients are $\phi = 0.7475$ and $\psi = 0.5218$.

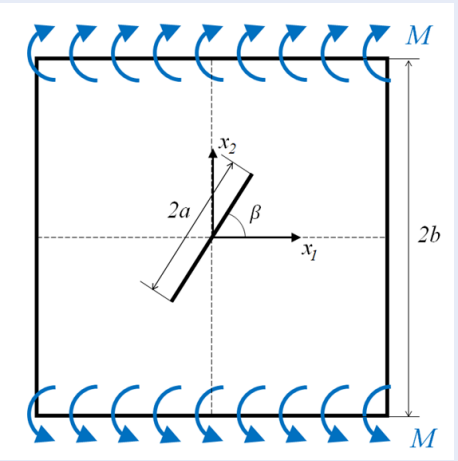

Figure 8: Square plate with a central slant crack under bending

Figure 9 shows the change of the intensity factors K_1 and K_2 due to the crack angle β. The figure shows that K_1 decreases when the orientation angle β increases, while K_2 increases and decreases symmetrically. It is also observed that the opening mode is dominant in the range of β from 0^0 to 40^0, and after that the magnitude of both SRIFs is approximate.

Figs 10 – 12 illustrate the distributions of normal stress σ_{11} and σ_{22}, and shear stress σ_{12}. The particular case for these figures is the inclined angle $\beta = 30^0$. The stress components are evaluated on the top surface of the plate. The stress singularity is clearly obtained at the crack tips.

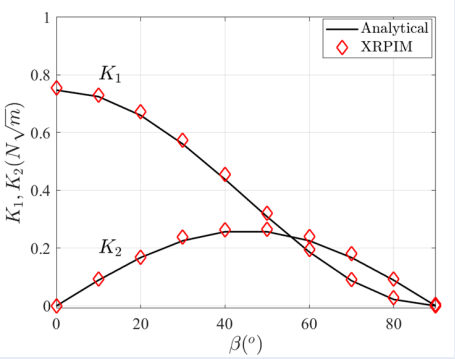

Figure 9: Variation of K_1 and K_2 versus the crack angle β

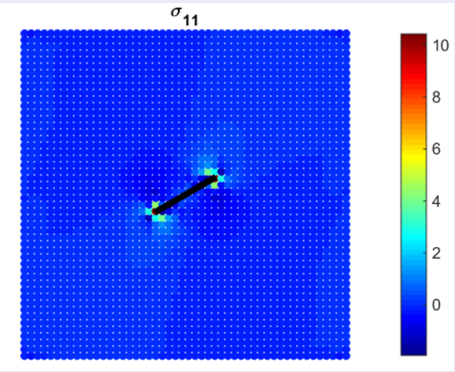

Figure 10: Normal stress distribution σ_{11} (Pa) on the top surface, $\beta = 30^0$.

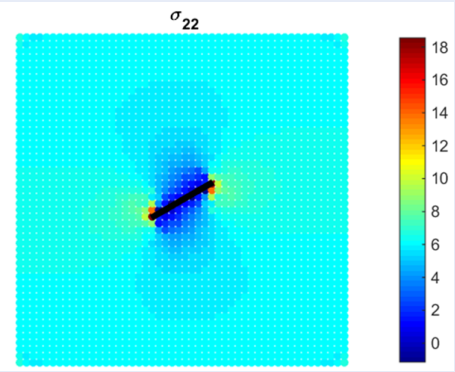

Figure 11: Distribution of normal stress σ_{22} (Pa) on the top surface, $\beta = 30^0$.

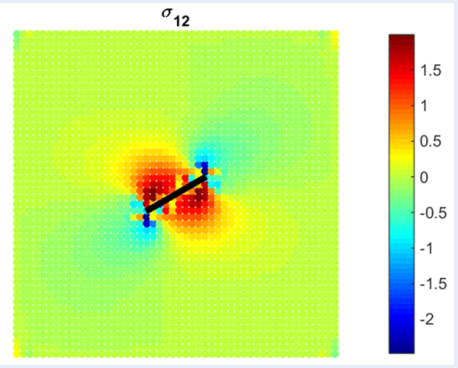

Figure 12: Distribution of shear stress σ_{12} (Pa) on the top surface, $\beta = 30^0$.

Transverse uniform pressure

The square plate with a horizontal central crack is subjected to transverse uniform pressure p. The boundary condition is simply supported on all edges, see Fig. 13. The material properties are: Young's modulus E=1000 Pa and Poisson ratio $v = 0.3$. The crack length is $2a$, and the ratio $b/t = 6$.

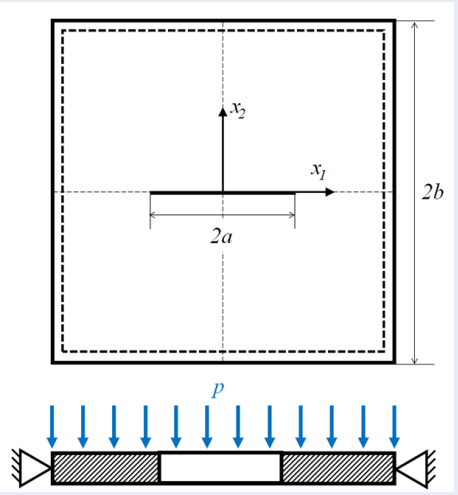

Figure 13: Simply supported square plate with central horizontal crack subjected to uniform pressure.

For horizontal crack, as shown in Fig. 9, K_2 is zero. Therefore, only K_1 is considered in this example. Figure 14 illustrates the variation of the normalized SRIF $K_1/\left(pb^2\sqrt{a}\right)$ with respect to ratios a/b. The obtained results by XRPIM are verified with the solution from the conventional FEM [25], showing good agreement. It can be observed from Fig. 14 that the SRIF tends to decrease as the a/b ratio increases. This trend as well

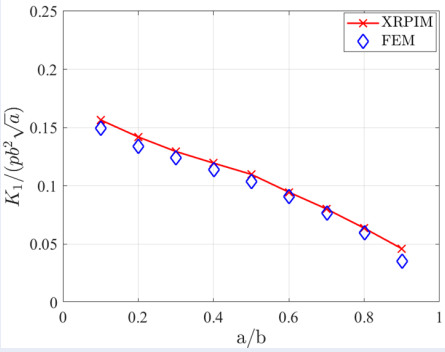

Figure 14: Normalized K_1 with different *a/b* ratios

as the slope of the curve is different from the example in Section 3.1. These two examples both have the same load, so the cause of this difference could be the boundary conditions. For the two cracks case, only two edges are simply supported while in this problem, all four edges are simply supported.

DISCUSSIONS

As presented in Section 3, the obtained results given by XRPIM are in good agreement with analytical solutions, FEM and DBEM. The trending variation of SRIFs is also observed from the numerical results. It can be remarked that the SRIFs depend on many factors: the number of cracks, crack orientation, load type and boundary conditions.

For the case of two cracks, the following conclusion can be drawn: the plate with higher thickness has higher SRIF, the SRIF decreases when the crack distance to plate length ratio *c/b* increases from 0.1 to 0.7, and after that the SRIF slightly increases when the *c/b* ratio is in the range of 0.7 – 0.9. It should be noted that a decrease in *c/b* ratio means an increase in the crack length, so the result can be interpreted as when the crack length increases, the SRIF also increases.

For the case of inclined crack, the result shows that K_1 decreases when the orientation angle β increases, while K_2 tends to increase and decrease symmetrically. It is also observed that the opening mode is dominant in the range of β from 0^0 to 40^0, and after that the magnitude of both SRIFs is approximate.

And for the case of horizontal crack under uniform pressure, the SRIF values decrease as the crack length to plate length ratio *a/b* increases. This decreasing trend is different from the two cracks example. These two examples both have the same uniform pressure, so the cause of this difference could be the boundary conditions. For the two cracks case, only two edges are simply supported while in the single horizontal crack problem, all four edges are simply supported.

CONCLUSIONS

Cracked plate problems are investigated in this study with the help of the extended meshfree XRPIM associated with the Reissner-Mindlin plate theory. The RPIM is different from other meshfree methods because it has the Kronecker delta property of shape functions. This property makes it easy to impose the essential boundary conditions in the RPIM as in the conventional FEM. The Reissner-Mindlin theory is suitable for the relatively thick plates due to the assumtion of first-order shear deformation. With a C^0 continuity formulation, it does not require higher-order shape functions. The present meshfree method would be possible to extend for complex cracked plate problems such as dynamic fracture, crack growth and nonlinear (geometry and material) analysis in future works.

The present approach is shown to be accurate in the evaluation of the stress resultant intensity factors. Many numerical examples show good agreement with analytical solutions and numerical solutions of other methods. The trend of SRIF in different cases is also observed.

ACKNOWLEDGMENT

This research is funded by Vietnam National University Ho Chi Minh City (VNU-HCM) under grant number B2022-20-02. We acknowledge the support of time and facilities from Ho Chi Minh City University of Technology (HCMUT), VNU-HCM for this study.

ABBREVIATIONS

DOF: Degree of freedom.
FEM: Finite Element Method.
FSDT: First-order shear deformation theory.
HSDT: Higher-order shear deformation theory.
RPIM: Radial Point Interpolation Method.
SIF: Stress intensity factor.
SRIF: Stress resultant intensity factor.
TPS: Thin Plate Spline.
XFEM: eXtended Finite Element Method.
XRPIM: eXtended Radial Point Interpolation Method.

CONFLICT OF INTEREST

Group of authors declare that this manuscript is original, has not been published before and there is no conflict of interest in publishing the paper.

AUTHORS' CONTRIBUTION

Vay Siu Lo is the main developer of the method and edits the manuscript.

Thien Tich Truong plays the role of the supervisor, he also contributes overall ideas for the proposed method.

Nha Thanh Nguyen contributes key idea for the proposed method and also checking the manuscript.

REFERENCES

1. Szilard R. Theories and applications of plate analysis. John Wiley & Sons, Inc; 2004;Available from: https://doi.org/10.1002/9780470172872.
2. D'Ottavio M, Polit O. Classical, first order, and advanced theories. In: Stability and vibrations of thin walled composite structures. Elsevier; 2017. p. 91-140;Available from: https://doi.org/10.1016/B978-0-08-100410-4.00003-X.
3. Bauchau OA, Craig JI. Kirchhoff plate theory. In: Structural analysis. Springer Netherlands; 2009. p. 819-914;Available from: https://doi.org/10.1007/978-90-481-2516-6_16.
4. Bhaskar K, Varadan Retd TK. Classical plate theory. In: Plates. John Wiley & Sons, Ltd; 2014. p. 11-32;Available from: https://doi.org/10.1002/9781118894705.ch2.
5. Reissner E. On the theory of bending of elastic plates. J Math Phys. 1944;23(1-4):184-91;Available from: https://doi.org/10.1002/sapm1944231184.
6. Hughes TJR, Tezduyar TE. Finite elements based upon mindlin plate theory with particular reference to the four-node bilinear isoparametric element. J Appl Mech. 1981;48(3):587-96;Available from: https://doi.org/10.1115/1.3157679.
7. Ye X, Zhang S, Zhang Z. A locking-free weak galerkin finite element method for reissner-mindlin plate on polygonal meshes. Comput Math Appl. 2020;80(5):906-16;Available from: https://doi.org/10.1016/j.camwa.2020.05.015.
8. Bitar I, Richard B. Mindlin-reissner plate formulation with enhanced kinematics: theoretical framework and numerical applications. Eng Fract Mech. 2020;225:106839;Available from: https://doi.org/10.1016/j.engfracmech.2019.106839.
9. Reddy JN. A simple higher-order theory for laminated composite plates. J Appl Mech. 1984;51(4):745-52;Available from: https://doi.org/10.1115/1.3167719.
10. Thai CH, Tran LV, Tran DT, Nguyen-Thoi T, Nguyen-Xuan H. Analysis of laminated composite plates using higher-order shear deformation plate theory and node-based smoothed discrete shear gap method. Appl Math Modell. 2012;36(11):5657-77;Available from: https://doi.org/10.1016/j.apm.2012.01.003.
11. Bhar A, Phoenix SS, Satsangi SK. Finite element analysis of laminated composite stiffened plates using FSDT and HSDT: A comparative perspective. Compos Struct. 2010;92(2):312-21;Available from: https://doi.org/10.1016/j.compstruct.2009.08.002.
12. Dolbow J, Moës N, Belytschko T. Modeling fracture in mindlin-Reissner plates with the extended finite element method. Int J Solids Struct. 2000;37(48-50):7161-83;Available from: https://doi.org/10.1016/S0020-7683(00)00194-3.
13. Li J, Khodaei ZS, Aliabadi MH. Dynamic dual boundary element analysis for cracked Mindlin plates. Int J Solids Struct. 2018;152-153:248-60;Available from: https://doi.org/10.1016/j.ijsolstr.2018.06.033.
14. Useche J. Fracture dynamic analysis of cracked Reissner plates using the boundary element method. Int J Solids Struct. 2020;191-192:315-32;Available from: https://doi.org/10.1016/j.ijsolstr.2020.01.017.
15. Lasry J, Renard Y, Salaün M. Stress intensity factors computation for bending plates with extended finite element method. Int J Numer Methods Eng. 2012;91(9):909-28;Available from: https://doi.org/10.1002/nme.4292.
16. Lasry J, Pommier J, Renard Y, Salaün M. eXtended finite element methods for thin cracked plates with Kirchhoff-love theory. Int J Numer Methods Eng. 2010;84(9):1115-38;Available from: https://doi.org/10.1002/nme.2939.
17. Singh SK, Singh IV, Mishra BK, Bhardwaj G, Singh SK. Analysis of cracked plate using higher-order shear deformation theory: asymptotic crack-tip fields and XIGA implementation. Comput Methods Appl Mech Eng. 2018;336:594-639;Available from: https://doi.org/10.1016/j.cma.2018.03.009.
18. Minh PP, Duc ND. The effect of cracks on the stability of the functionally graded plates with variable-thickness using HSDT and phase-field theory. Compos B Eng. 2019;175:107086;Available from: https://doi.org/10.1016/j.compositesb.2019.107086.
19. Moes N, Dolbow J, Belytschko T. A finite element method for crack growth without remeshing. Int J Numer Methods Eng. 1999;46(1):131-50;Available from: https://doi.org/10.1002/(SICI)1097-0207(19990910)46:1<131::AID-NME726>3.0.CO;2-J.
20. Liu GR, Gu YT. A point interpolation method for two-dimensional solids. Int J Numer Methods Eng. 2001;50(4):937-51;Available from: https://doi.org/10.1002/1097-0207(20010210)50:4<937::AID-NME62>3.0.CO;2-X.
21. Liu Y, Y. C. Hon and . M. Liew, "A meshfree Hermite-type radial point interpolation method for Kirchhoff plate problems,". Int J Numer Methods Eng. 2006;66:1153-78;Available from: https://doi.org/10.1002/nme.1587.
22. Nguyen NT, Bui TQ, Zhang C, Truong TT. Crack growth modeling in elastic solids by the extended meshfree galerkin radial point interpolation method. Eng Anal Bound Elem. 2014;44:87-97;Available from: https://doi.org/10.1016/j.enganabound.2014.04.021.
23. Nguyen NT, Bui TQ, Truong TT. Transient dynamic fracture analysis by an extended meshfree method with different crack-tip enrichments. Meccanica. 2017;52(10):2363-90;Available from: https://doi.org/10.1007/s11012-016-0589-6.
24. Nguyen NT, Bui TQ, Nguyen MN, Truong TT. Meshfree thermo-mechanical crack growth simulations with new numerical integration scheme. Eng Fract Mech. 2020;235:107-21;Available from: https://doi.org/10.1016/j.engfracmech.2020.107121.
25. Sosa HA, Eischen JW. Computation of stress intensity factors for plate bending via a path-independent integral. Eng Fract Mech. 1986;25(4):451-62;Available from: https://doi.org/10.1016/0013-7944(86)90259-6.
26. Ferreira AJM, Fantuzzi N. MATLAB codes for finite element analysis. Solid Mech Appl. 2020;Available from: https://doi.org/10.1007/978-3-030-47952-7.
27. Liu GR. Meshfree methods: moving beyond the finite element method. Boca Raton: CRC Press; 2010;.
28. Truong TT, Lo VS, Nguyen MN, Nguyen NT, Nguyen DK. Evaluation of fracture parameters in cracked plates using an extended meshfree method. Eng Fract Mech. 2021;247:107671;Available from: https://doi.org/10.1016/j.engfracmech.2021.107671.
29. Boduroglu H, Erdogan F. Internal and edge cracks in a plate of finite width under bending. J Appl Mech. 1983;50(3):621-9;Available from: https://doi.org/10.1115/1.3167100.
30. Dirgantara T, Aliabadi MH. Dual boundary element formulation for fracture mechanics analysis of shear deformable shells. Int J Solids Struct. 2001;38(44-45):7769-800;Available from: https://doi.org/10.1016/S0020-7683(01)00097-X.
31. Sih GC. Strain energy density theory applied to plate-bending and shell problems. In: Mechanics of fracture initiation and propagation. Springer Netherlands; 1991. p. 57-98;Available from: https://doi.org/10.1007/978-94-011-3734-8_3.
32. Delate F, Erdogan F. The effect of transverse shear in a cracked plate under skew-symmetric loading. J Appl Mech. 1979;46(3):618-24;Available from: https://doi.org/10.1115/1.3424616.

Tạp chí Phát triển Khoa học và Công nghệ – Engineering and Technology 2023, 5(SI2):24-32

Open Access Full Text Article

Bài nghiên cứu

Phân tích tấm nứt Reissner-Mindlin bằng một phương pháp không lưới mở rộng

Lồ Sìu Vẫy[1,2], Trương Tích Thiện[1,2], Nguyễn Thanh Nhã[1,2,*]

TÓM TẮT

Bài báo này trình bày một phương pháp không lưới mở rộng để phân tích các tấm nứt dựa trên lý thuyết tấm Reissner-Mindlin. Trong các phương pháp không lưới, phương pháp nội suy điểm hướng kính (RPIM) được chọn trong nghiên cứu này do sự thỏa mãn thuộc tính Kronecker delta. Do đó, các điều kiện biên cần thiết có thể được áp đặt dễ dàng trong RPIM. Hàm dạng RPIM được sử dụng để nội suy chuyển vị và các biến môi trường trong bài toán. Phương pháp RPIM mở rộng được sử dụng để mô hình vết nứt mà không cần mô tả tường minh nó trong miền rời rạc của bài toán. Sự bất liên tục gây ra bởi vết nứt được xác định bằng các hàm làm giàu, cụ thể là, bước nhảy trong trường chuyển vị trên hai mặt của vết nứt được mô hình hóa bằng hàm Heaviside và sự suy biến ứng suất gần đỉnh vết nứt được mô tả bằng hàm làm giàu tiệm cận đỉnh vết nứt. Trong nghiên cứu này, các hệ số cường độ ứng suất tổng hợp (SRIFs) được đánh giá thông qua phương pháp tích phân tương tác. Xu hướng biến thiên của SRIFs cũng được xem xét trong các kết quả tính toán số. Có thể nhận xét rằng SRIFs phụ thuộc vào nhiều yếu tố: số lượng vết nứt, định hướng của vết nứt, loại tải trọng và điều kiện biên. Các kết quả SRIFs thu được trong bài báo được trình bày thông qua nhiều ví dụ số nhằm mục đích so sánh và kiểm chứng độ chính xác của phương pháp. Kết quả thu được được so sánh với các kết quả giải tích và các phương pháp số khác.

Từ khoá: tấm nứt, tấm Reissner-Mindlin, phương pháp không lưới mở rộng, XRPIM

[1]*Bộ môn Cơ kỹ thuật, Khoa Khoa học ứng dụng, Trường Đại học Bách khoa Tp. HCM, Việt Nam*

[2]*Đại học Quốc gia Thành phố Hồ Chí Minh, Việt Nam*

Liên hệ

Nguyễn Thanh Nhã, Bộ môn Cơ kỹ thuật, Khoa Khoa học ứng dụng, Trường Đại học Bách khoa Tp. HCM, Việt Nam

Đại học Quốc gia Thành phố Hồ Chí Minh, Việt Nam

Email: nhanguyen@hcmut.edu.vn

Lịch sử

- Ngày nhận: 16-12-2022
- Ngày chấp nhận: 24-8-2023
- Ngày đăng: 31-12-2023

DOI : https://doi.org/10.32508/stdjet.v6iSI2.1066

VNUHCM PRESS

Trích dẫn bài báo này: Vẫy L S, Thiện T T, Nhã N T. **Phân tích tấm nứt Reissner-Mindlin bằng một phương pháp không lưới mở rộng** . *Sci. Tech. Dev. J. - Eng. Tech.* 2023, 5(SI2):24-32.